

Meteorological factors and non-pharmaceutical interventions explain local differences in the spread of SARS-CoV-2 in Austria

Katharina Ledebur^{1,2}, Michaela Kaleta^{1,2}, Jiaying Chen^{1,2,3}, Simon Lindner^{1,2}, Caspar Matzhold^{1,2}, Florian Weidle⁴, Christoph Wittmann⁴, Katharina Habimana⁵, Linda Kerschbaumer⁵, Sophie Stumpfl⁵, Georg Heiler^{2,6}, Martin Bicher^{6,7}, Nikolas Popper^{6,7,8}, Florian Bachner⁵, Peter Klimek^{1,2,*}

¹*Medical University of Vienna, Section for Science of Complex Systems, CeMSIIS, Spitalgasse 23, 1090 Vienna, Austria;*

²*Complexity Science Hub Vienna, Josefstädter Straße 39, 1080 Vienna, Austria;*

³*Division of Insurance Medicine, Department of Clinical Neuroscience, Karolinska Institutet, SE-171 77, Stockholm, Sweden;*

⁴*Zentralanstalt für Meteorologie und Geodynamik, Hohe Warte 38, 1190 Vienna, Austria;*

⁵*Austrian National Public Health Institute, Stubenring 6, A-1010 Vienna, Austria;*

⁶*Institute of Information Systems Engineering, TU Wien, Favoritenstraße 8-11, A-1040 Vienna, Austria;*

⁷*dwh simulation services, dwh GmbH, Neustiftgasse 57-59, A-1070 Vienna, Austria;*

⁸*Association for Decision Support Policy and Planning, DEXHELPP, Neustiftgasse 57-59, A-1070 Vienna, Austria.*

*Correspondence: peter.klimek@meduniwien.ac.at

21 **The drivers behind regional differences of SARS-CoV-2 spread on finer spatio-temporal**
22 **scales are yet to be fully understood. Here we develop a data-driven modelling approach**
23 **based on an age-structured compartmental model that compares 116 Austrian regions to a**
24 **suitably chosen control set of regions to explain variations in local transmission rates through**
25 **a combination of meteorological factors, non-pharmaceutical interventions and mobility. We**
26 **find that more than 60% of the observed regional variations can be explained by these factors.**
27 **Decreasing temperature and humidity, increasing cloudiness, precipitation and the absence**
28 **of mitigation measures for public events are the strongest drivers for increased virus trans-**
29 **mission, leading in combination to a doubling of the transmission rates compared to regions**
30 **with more favourable weather. We conjecture that regions with little mitigation measures for**
31 **large events that experience shifts toward unfavourable weather conditions are particularly**
32 **predisposed as nucleation points for the next seasonal SARS-CoV-2 waves.**

33 1 Introduction

34 The SARS-CoV-2 pandemic impacted different world regions in a highly heterogeneous way. A
35 vast body of research has sought to explain these differences by factors ranging from varying
36 stringency of non-pharmaceutical interventions (NPIs)¹⁻⁴, socio-economic and demographic factors
37⁵⁻⁷ to different virus variants.^{8,9} Relatively less attention has been paid to more fine-scaled spatio-
38 temporal variations in virus spread.^{10,11} Next to regional differences in NPIs, meteorological¹²⁻¹⁷
39 and behavioural factors have been proposed to account for such variations.¹⁸⁻²¹ Infection waves
40 typically start with localized outbreaks in specific regions before case numbers start to soar on
41 larger geographic scales.²² Such localized outbreaks are often initiated by singular events in which
42 transmission is dominated by a small number of individuals,^{23,24} so-called superspreading events.
43²⁵ As these events are stochastic and therefore near-impossible to predict, the question arises to
44 which extent fine-scaled spatio-temporal variations can actually be explained or whether they are
45 irreducibly random.

46 Here we seek to understand the factors that determine on finer geographic scales the degree
47 to which the infection dynamics in one region in Austria deviated from the dynamics observed
48 in neighboring regions. We consider factors from three different domains to account for these
49 variations, namely meteorology (temperature, cloudiness, humidity, precipitation, wind), non-
50 pharmaceutical interventions (targeting schools, gastronomy, healthcare, or events) as well as
51 individual-level mobility (as inferred from telecommunications data).

52 Previous literature reported inconsistent associations of weather with transmission dynamics,

53 ¹²⁻¹⁷ suggesting that the assessment of the impact of meteorological factors might depend on
54 geography, epidemic phase and the spatio-temporal scale on which the analysis is conducted. In this
55 work, we use meteorological forecast data derived from the mesoscale numerical weather model
56 AROME (Application of Research to Operations at Mesoscale ^{26,27}) to quantify regional weather
57 related factors. AROME is operated by ZAMG (Zentralanstalt für Meteorologie und Geodynamik)
58 for a domain covering the Alpine area. More details are given in section. 2

59 The literature is more consistent with regard to the transmission-reducing effects of restricted
60 mobility. ¹⁸⁻²¹ However, such effects cannot be fully disentangled from the effects of physical dis-
61 tancing policies. ²⁸ For Austria it was observed that the same regime of governmental interventions
62 induced quite heterogeneous mobility changes across regions. ²⁹ Here we measure mobility by
63 means of the median Radius of Gyration of cell phone users in a region, which is a measure for the
64 daily area travelled by these users.

65 In autumn 2020, Austria adopted a tiered pandemic management plan in which each region
66 was assigned one of four alert levels (green, yellow, orange, red) signalling its epidemiological
67 risk. ³⁰ The assessment was performed based on a set of indicators including confirmed cases,
68 available hospital capacities and the functionality of contact tracing. Regional authorities decided
69 on appropriate response measures in reaction to the weekly risk assessment, meaning that the same
70 alert level could and did translate into different NPIs across regions. We used an extensive dataset on
71 all regional response measures in Austria curated by the Austrian National Public Health Institute.
72 We clustered the response measures into four different categories, based on whether they affect

73 schools (bans on singing in class rooms, cloth masks when not seated, ...), gastronomy (limits for
74 the number of persons allowed to share a table, opening hours, ...), healthcare settings (e.g., visitor
75 bans), or events (size restrictions).

76 Our methodological approach is outlined in Fig. 1. There we show a map of Austria divided
77 into its nine federal states. The state of Tyrol (blue) is further divided into its finer administrative
78 regions of districts. In Fig. 1 we show the epidemiological curve observed in the district of Innsbruck
79 (orange) and compare it with two models. First, we compare it to results from an age-structured
80 compartmental model that assumes the infection rate observed in Innsbruck (orange) to be the
81 same as the rate observed in all other districts taken together in the same federal state (blue, the
82 control set for the orange district), giving the red epidemiological curve. Second, we augment this
83 model by assuming that the age-dependent transmission rates are also a function of the district-level
84 meteorological, intervention and mobility time-series with district-independent effect sizes learned
85 from data by means of a cross-validated nonlinear least squares solver. This approach provides us
86 with estimates for the effect of each of the ten input time series on regional virus spread and for the
87 degree to which the combined effects of weather, interventions and individual-level mobility can be
88 used to explain differences in the spread between regions.

89 **2 Data and Methods**

90 **Case data.** Our study period ranges from July 1 2020 to May 15 2021. The daily confirmed
91 Covid-19 cases of 116 districts in Austria were collected through the official Austrian COVID-19

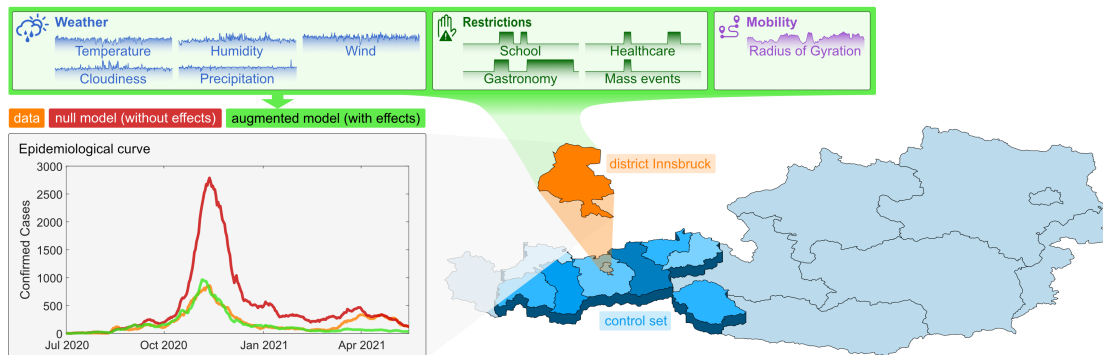


Figure 1: Visual representation of the methodological approach. For every one of the 116 districts in Austria the epidemiological curve of the district is compared to the epidemiological curve of the corresponding federal state. This figure shows the example of the district Innsbruck (orange) in the federal state Tyrol. The epidemiological curves are calculated employing an age-structured compartmental model. The red curve is the epidemiological curve for Innsbruck assuming transmission rates that equal those observed in Tyrol (blue). By including a dependence of the transmission rate on weather, interventions and mobility (green), the district-independent effect sizes of these district-specific input variables can be calculated.

92 disease reporting system (EMS) ³¹. A unique identification number was assigned to each positive
93 Covid-19 test. People can be tested positive multiple times. We calculate daily numbers of positive
94 tests per district and age group. The population size per district was available from the national
95 statistics office and linked by the unique district ID.

96 **Meteorological data.** We further used detailed information on the weather situation in Austria,
97 including gridded forecast data on five meteorological parameters: total cloudiness, precipitation,
98 2m temperature, 2m relative humidity and 10m wind speed. The gridded data sets were provided by
99 the mesoscale weather model AROME operated at ZAMG eight times per day producing forecasts
100 up to 60 hours ahead. AROME is a spectral limited area model currently operating on a 2.5km
101 horizontal grid covering the Alpine area using 90 vertical levels up to a height of approximately
102 35hPa. The 3D atmospheric initial conditions for the model runs are created using a variational data
103 assimilation system (3DVAR, ³²) which is fed by a large number of observations (surface station
104 data, radiosondes, satellite data, aircraft data, etc.). To derive the surface initial conditions, an
105 optimum interpolation method is implemented.

106 For this study, the meteorological model data is provided for the study period on an hourly
107 basis. The gridded AROME data was further aggregated to create information on a district level,
108 where the district value of an input time series is given by the population-weighted average of
109 the values observed in the corresponding grid cells. We calculate the daily mean values of these
110 parameters in each district and subtract the mean value of the daily mean values of all other districts
111 in the same federal state (control set) as input for the model.

112 **Data on regional NPIs.** A dataset on regional Austrian NPIs was collected and curated by the
 113 Austrian National Public Health Institute. This data contains precise information on federal state,
 114 district, type and details of intervention, start and end date of registered regional measures. The data
 115 set contains 11 individual types and an additional 83 subtypes of interventions. We further grouped
 116 these types and subtypes of NPIs into 4 larger groups of restrictions: 1) restrictions in schools, 2)
 117 restrictions in gastronomy, 3) restrictions in healthcare, 4) restrictions for larger events. Intervention
 118 measures dependent on the corona traffic light were matched to the districts in appropriate traffic
 119 light colors in the given time frame. For each day in the observed time period and each district we
 120 assigned binary values of true/false for each intervention group.

121 **Mobility data.** The mobility data contains 1,683,270 entries, including information on the date
 122 of travel, regions by postal code (which were mapped to districts), the number of devices in
 123 this particular region, and the radius of gyration over the study period. For each region only
 124 k-anonymized data is available. Any region with less than k unique devices on a specific day is
 125 redacted. The radius of gyration is defined as the square root of the time-weighted centroid of
 126 the squared distances of the mobility events (locations) $\vec{x}_{i\mu}$ to the most prominent location (night
 127 location, center of mass) $\bar{x}_i = \frac{\sum_{\mu} \vec{x}_{i\mu} t_{i\mu}}{\sum_{\mu} t_{i\mu}}$ of each day:

$$R_{G,i} = \sqrt{\frac{\sum_{\tau} d(\bar{x}_i, \vec{x}_{i\tau})^2}{\sum_{\tau} t_{i\tau}}} \quad (1)$$

128 Finally, as input time series for the model we consider the logarithmic radius of gyration and subtract
 129 the average logarithmic radius of gyration observed in the control set.

130 **Regional age-structured SIR null model without effects** To identify the impact of meteorologi-
 131 cal factors, mitigation strategies and mobility on the infection dynamics across Austria, the epidemic
 132 curves of the 116 districts of Austria are compared. We employ a parsimonious age-structured SIR
 133 model³³ to facilitate robust calibration.

134 Our approach makes use of the fact that when the confirmed cases per day are known, the
 135 “effective” transmission rate α can be calculated from data alone within the SIR model. For each
 136 district b , we compute a transmission rate for day n and age group a in the null model (without
 137 effects), $\alpha_{n,a}^0(b)$, as follows. Our null hypothesis is that the epidemiological curve of a given district
 138 b (shown as orange in Fig. 1) has values of $\alpha_{n,a}^0(b)$ that are identical to the transmission rate observed
 139 in all other districts of the same federal state (blue in Fig. 1). We call these districts the control set
 140 of districts for b , \mathcal{C}_b . For this control set we observe the time series of cumulative confirmed cases,
 141 $C_{n,a}(\mathcal{C}_b)$.

142 Let $S(\mathcal{C}_b)$, $I(\mathcal{C}_b)$, $R(\mathcal{C}_b)$, and $N(\mathcal{C}_b)$ be the daily numbers of susceptible, infected, recovered
 143 and total number of people in the control set, respectively. We have,

$$\alpha_{n,a}(\mathcal{C}_b) = \frac{(C_{n+1,a}(\mathcal{C}_b) - C_{n,a}(\mathcal{C}_b)) N_a(\mathcal{C}_b)}{S_{n,a}(\mathcal{C}_b) \sum_{a'} c_{aa'} I_{n,a'}(\mathcal{C}_b)}, \quad (2)$$

144 where $c_{aa'}$ represents social mixing by age. We compute a social mixing matrix for every
 145 district to define the number of infected individuals a susceptible individual from one age group
 146 is exposed to. The social mixing matrix by age for Austria is obtained from Prem *et al.* (2017)
 147³⁴ with the population being grouped into four age brackets (0-19, 20-39, 40-64 and 65+ year old

148 individuals). We calculate a social mixing matrix for every district and federal state. To calculate
 149 the social mixing matrix entry for one of the four new age groups, we build the population-weighted
 150 sum over the corresponding social mixing matrix entries provided by Prem *et al.* (2017). The
 151 social mixing matrices for each federal state (used for the control sets) are again given by the
 152 population-weighted sum over the individual districts.

153 The number of susceptible, infected and removed individuals in one of the four age groups a ,
 154 can be calculated for the control set as,

$$S_{n+1,a}(\mathcal{C}_b) = S_{n,a}(\mathcal{C}_b) (1 - \lambda_{n,a}(\mathcal{C}_b)) \quad (3)$$

$$I_{n+1,a}(\mathcal{C}_b) = I_{n,a}(\mathcal{C}_b) + \lambda_{n,a}(\mathcal{C}_b)S_{n,a}(\mathcal{C}_b) - \beta I_{n,a}(\mathcal{C}_b) \quad (4)$$

$$R_{n+1,a}(\mathcal{C}_b) = R_{n,a}(\mathcal{C}_b) + \beta I_{n,a}(\mathcal{C}_b) \quad , \quad (5)$$

155 where we defined $\lambda = \frac{\alpha_{n,a}(\mathcal{C}_b)}{N_a(\mathcal{C}_b)} \sum_{a'} c_{aa'} I_{n,a'}(\mathcal{C}_b)$. Initial conditions are given by $I_{0,a}$ as the day with
 156 the first case(s) in age group a and $S_{0,a} = 1 - I_{0,a}$.

157 The null model (without effects) for district b can then be obtained by assuming that

$$\alpha_{n,a}^0(b) = \alpha_{n,a}(\mathcal{C}_b) \quad \forall n, a, b \quad , \quad (6)$$

158 holds for an age-structured SIR model for district b .

159 **Augmented regional model with effects** To quantify the impact of meteorological factors, mitiga-
 160 tion strategies and overall mobility on the epidemic curves of all districts in Austria, we augment
 161 the null model in the following way.

162 In total we consider 10 input time series $X_n(b, i)$, $i = 1, \dots, 10$. The NPI time series
 163 contain binary variables, $X_n(b, i) \in \{0, 1\}$, indicating whether a given measure was implemented
 164 in the region or not. For the meteorological and mobility time series the input signal is given
 165 by the deviation of $X_n(b, i)$ between the district and its control set, i.e., we map $X_n(b, i) \rightarrow$
 166 $X_n(b, i) - \langle X_n(b', i) \rangle_{b' \in \mathcal{C}_b}$ where $\langle \cdot \rangle_{b' \in \mathcal{C}_b}$ denotes the arithmetic average over all districts in the
 167 control set. To each input time series we assign an effect on the transmission rate by assuming that

$$\alpha_{n,a}(b) = \alpha_{n,a}^0(b) \prod_{i=1}^{10} (1 + \alpha_a(i) X_n(b, i)) \quad , \quad (7)$$

168 such that $\alpha_a(i)$ quantifies by how many percent changes in the input time series impact on the
 169 transmission rate. We further assume that $\alpha_a(i) \equiv \alpha(i)$ (i.e., effects are not age-dependent) for all
 170 input time series except NPIs related to schools, for which we assume an effect size in the first age
 171 group ($< 20y$) that is different from all other age groups. Observe that $\alpha(i)$ are district-independent
 172 effects.

173 **Hyperparameter search and cross-validation** We solve the models for $\alpha(i)$ by means of a
 174 Levenberg-Marquandt (LM) algorithm optimizing the residual sum of squares (RSS) between
 175 age-specific incidence time series in data and model; incidence is measured as fraction of the total
 176 population. The model has one remaining hyperparameter, namely the recovery rate β . To fix β ,
 177 we perform a cross-validated hyperparameter search over the range $1/\beta = 4, \dots, 35d$. We perform
 178 randomized cross-validation by splitting the time series into blocks of 28d and randomly picking
 179 80% of these blocks for training (fitting $\alpha(i)$ via LM) and evaluating the RSS on the remaining 20%
 180 test data. We then choose β such that the difference in RSS between null and augmented model is
 181 maximized by means of the elbow method. To obtain the effect sizes we finally evaluate the model

182 on the full dataset.

183 **3 Results**

184 **Model calibration.** Results for the cross-validated hyperparameter search to fix the recovery time,
185 β , are shown in Fig. 2. The larger the recovery time, the higher the percentage of regional variations
186 that the augmented model is able to explain with respect to the null model. For recovery times of
187 $>20d$, the explained variation saturates at a bit more than 60%. Values for the training data are only
188 marginally higher than for the test data, suggesting that overfitting is not much of an issue. In the
189 following, we fix β to 25d.

190 **Effect sizes.** Results for the effect sizes of meteorological, intervention and mobility variables
191 are shown in Fig. 3. Confidence intervals are obtained from a 100-fold cross-validation. For the
192 continuous variables (weather, mobility), see Tab. 1, we report the percent change in transmission
193 rates in units of one standard deviation (SD) of the variable in the district with respect to its control
194 set of districts. All meteorological variables show a significant effect. Strong effects can be observed
195 for humidity, where one SD decreases the transmission rate by 17.1% (95%CI $-17.3, -16.9$), as
196 well as for cloudiness and precipitation, where one SD increases transmission rates by 15.5%
197 (95%CI $-15.2, -15.8$) and 18.9% (95%CI $-18.4, -19.5$) respectively. The transmission rate is
198 also inversely associated with temperature, while wind slightly increases transmissions. Mobility, as
199 measured by the logarithmic radius of gyration, increases transmissions by 7.7% (95% CI 7.4, 8.0).

200 Considering the NPIs, restrictions targeting mass events show the strongest effect on trans-

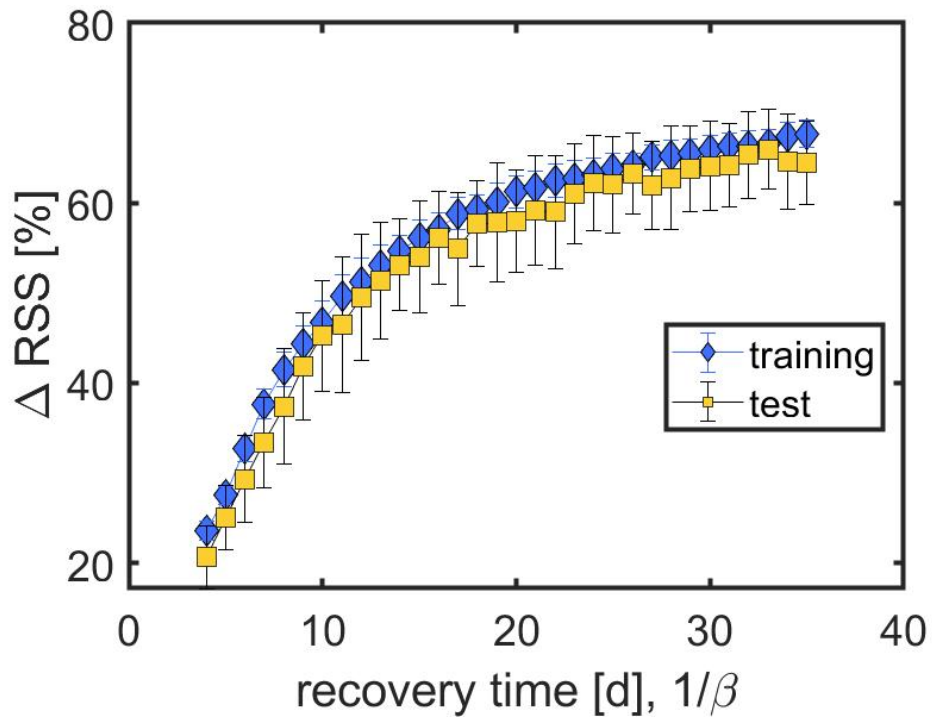


Figure 2: Results for the cross-validated hyperparameter search. For different recovery times, $1/\beta$, we show the percent change in RSS, ΔRSS , between null and augmented model for training (blue) and test (yellow) data. For recovery times of more than 20d, the augmented model explains more than 60% of the regional variations in both test and training data.

201 missions with reductions of about 40%, see also Tab. 2. Restrictions in healthcare settings and
202 gastronomy reduce transmissions by about 20%, respectively. For school measures we observe
203 age-dependent effects. While restrictions for schools reduced transmissions by about 8% in the
204 population younger than 20y, we observe no significant impact of school measures on older age
205 groups.

206 **4 Discussion**

207 In this work we aimed to understand the extent to which fine-scaled spatio-temporal variations in
208 the spread of SARS-CoV-2 can be explained by differences in meteorological factors, NPIs, or
209 mobility. We assume that deviations in time- and age-dependent transmission rates of a district from
210 the transmission rate in other districts of the same federal state result from different temperatures,
211 cloudiness, humidity, precipitation, wind, mobility, or measures targeting schools, gastronomy,
212 healthcare or mass events. We found that taken together these factors account for more than 60%
213 of the variation observed in regional transmission. Humidity, cloudiness and precipitation turned
214 out to be the dominating meteorological factors, and restrictions targeting mass events showed the
215 greatest reduction in local transmission.

216 As our approach aims to minimize the quadratic distance between data and model incidences,
217 the model is optimized to explain the data in pandemic phases of high incidence. Fig. 1 shows this
218 overall tendency in that the augmented model fits the first peak (Nov 2020) substantially better than
219 the second peak (April 2021). Austria experienced its highest incidences within the study period in

variable	unit	SD	transmission rate change [%]
temperature	$^{\circ}C$	2.4	-6.9 (-7.1, -6.8)
cloudiness	[0-1]	0.11	15.5 (15.2, 15.8)
humidity	[0-1]	0.063	-17.1 (-17.3, -16.9)
precipitation	mm/h	0.21	19.0 (18.4, 19.5)
wind	m/s	0.95	3.0 (2.9, 3.1)
log. radius of gyration	m	7.9	7.7 (7.4, 8.0)

Table 1: Summary of effects of meteorological and mobility time series on the transmission rate. For each variable we give its unit, the standard deviation (SD) of the input time series and the percent change with its 95% confidence intervals of the transmission rate associated with a unit SD change in the input.

category	N	examples	transmission rate change [%]
schools	144	cloth masks when entering schools, no indoor singing, sports only outdoors, measures to avoid mixing of school classes, ...	$< 20y$: -7.9 ($-10.6, -5.1$) $\geq 20y$: 0.7 ($-0.1, 1.5$)
gastronomy	123	closing time at 10pm, limits for number of people seated at table, mandatory registration, ...	-18 ($-17, -19$)
healthcare	161	visitor ban or a maximum of one visitor per week, mandatory registration, FFP2 masks, ...	-20.6 ($-21.2, -20.1$)
events	69	ban or size limits of seated and un-seated indoor and outdoor events	-37.5 ($-38.6, -36.5$)

Table 2: Summary of effects of NPIs on the transmission rate. For each category of NPIs we give the number of implementations observed in our data, list typical examples of what the NPI consists of and the percent change of the transmission rate associated with a unit SD change in the input.

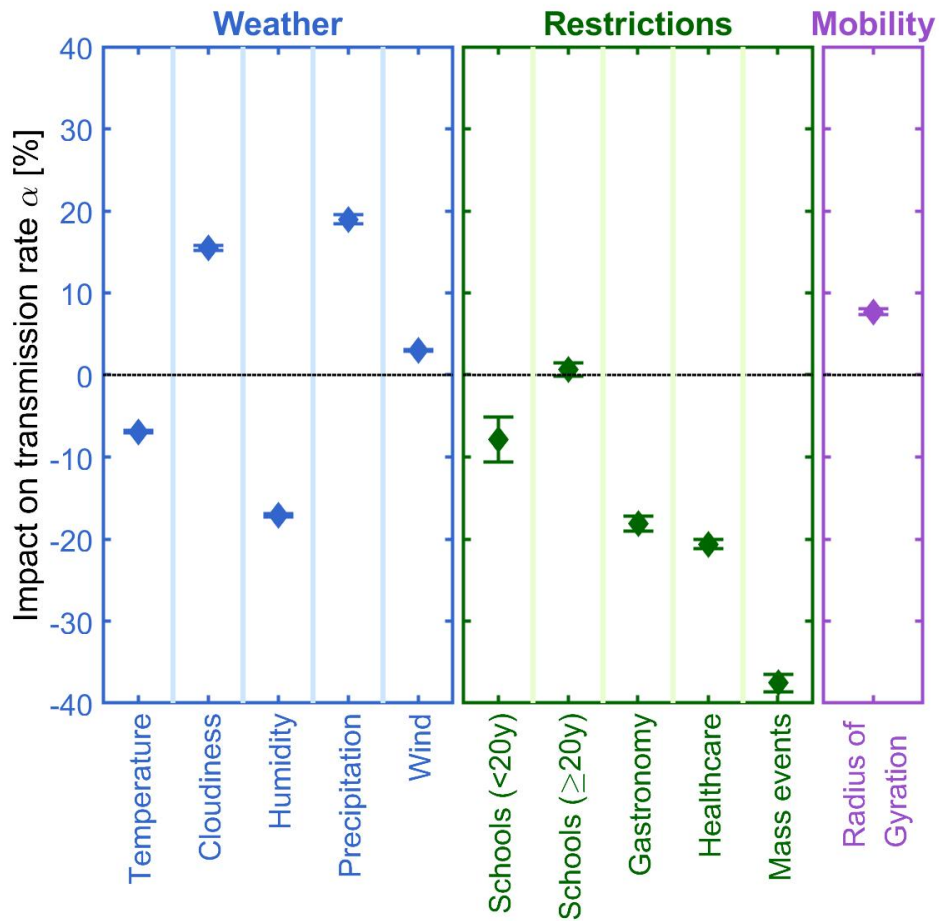


Figure 3: Summary of effect sizes of NPIs. Impacts on the transmission rate are shown in percent for weather variables (blue), NPIs (green) and mobility (magenta). Results for weather and mobility timeseries refer to changes in α for a unit change of one SD in the input. NPIs targeting large gatherings, temperature and humidity show the strongest transmission rate reductions whereas cloudiness leads to the strongest increase. Error bars denote the CI.

220 most districts in November 2020, when the Austrian 7-day-incidence per 100,000 reached values of
221 above 500. Our effect estimates are therefore particularly valid to describe the factors that might
222 explain why certain districts were more (e.g., the district Rohrbach with a maximal 7-day-incidence
223 of more than 1,500) or less (e.g., Gänserndorf where the incidence peaked at about 240) affected in
224 the growth phase of this wave, i.e. the early growth behaviour of the 2020 seasonal SARS-CoV-2
225 wave. Note that here we do not address factors that impact the spread of SARS-CoV-2 in all districts
226 of a federal state homogeneously, such as NPIs that were implemented on national scales, seasonal
227 influences (as opposed to fine-scaled weather influences), or dominant virus variants.

228 Previous literature reported inconsistent associations of weather with transmission dynamics.
229 ¹²⁻¹⁷ For instance, analysis of an early outbreak in China found a positive association of the infection
230 rate with temperature, ¹² as did a correlation study in Norway. ¹³ whereas an analysis for Spain ¹⁷
231 and a meta-analysis of 202 locations in 8 countries ¹⁵ observed no significant correlation. On the
232 other hand, for the US ¹⁶ and another early, multi-city study in China ³⁵ negative associations were
233 reported. Also regarding the other meteorological factors the literature reports contrary results. The
234 previously mentioned analysis of an early outbreak in China ¹² reports that increase in humidity
235 and precipitation enhances the number of confirmed cases whereas the multi-city study in China ³⁵
236 reports that low humidity likely favors the transmission of Covid-19. Additionally, the correlation
237 study in Norway ¹³ stated that precipitation is negatively related with Covid-19 cases. Wind may be
238 a crucial factor in the spread of infectious diseases. ³⁶ Several studies had examined the relation
239 of wind speed and the transmission of coronavirus and showed heterogeneous effects in different
240 countries. ^{13,37} Nevertheless, an observational study using data from 190 countries suggested an

241 inverse association of wind speed with transmission.³⁸

242 The reasons for this divergence in the literature regarding meteorological influences are not
243 entirely clear. The studies mentioned above differ greatly in the included covariates, methodological
244 approaches as well as geographic and temporal scales on which the analysis was performed,
245 which all hinders comparability. A nonlinear dependence on temperature has also been proposed
246 for the transmission rate.³⁹ In our study that adjusts for larger-scale regional trends, regional
247 response measures and mobility we observe that increases in temperature and humidity both and
248 independently lead to decreased transmission rates. These findings are in line with results from
249 studies showing that higher temperature and humidity both lead to faster inactivation of SARS-CoV-
250 2 on surfaces and in aerosols.^{40–42} Airborne SARS-CoV-2 is also known to be rapidly inactivated
251 by sunlight^{43–45}, in line with our finding that transmission rates increase with cloudiness.

252 Meteorological factors might impact SARS-CoV-2 transmission also through behavioural
253 effects. For example, it is feasible that people prefer to meet inside rather than outside during rainy
254 days which leads to an increase in COVID-19 cases.

255 A recent meta-analysis found that school closing was the most effective NPI in reducing the
256 spread of SARS-CoV-2, followed by workplace closing, business closing and public event bans.
257 ⁴⁶ The school measures evaluated here were substantially less disruptive than full closures and
258 included “soft” restrictions such as bans in indoor singing and sport activities, the requirement
259 to wear a cloth mask when entering or leaving the school building (but not when seated in the
260 class room), or measures to mitigate contacts between pupils from different classes. We find that

261 such less disruptive measures nevertheless coincided with significantly reduced transmission rates
262 in the age group $< 20y$ by about -7.9% ($-10.6, -5.1$). Our finding of a non-significant effect
263 of school measures on transmission rates in age groups above $20y$ should not be interpreted to
264 mean transmissions in school settings are decoupled from the population-level spread. Rather,
265 transmission rates in older population groups are indirectly impacted by school measures in our
266 model through the age-structured social mixing matrices.

267 Regarding gastronomy, we again note that our analysis focuses on less disruptive measures
268 that did not consist of full closures, but rather of restrictions such as mandatory registration of
269 visitors, limits for the opening hours or for the number of people seated at a table. While the
270 effectiveness of fully closing such venues has been repeatedly established in the literature,⁴⁶ it is
271 maybe surprising to note that less disruptive interventions also coincide with noticeably reduced
272 transmission rates by about -18% ($-17, -19$).

273 Measures targeting the healthcare sector such as visitor bans and mandatory FFP2 masks
274 showed a stronger effect than the less disruptive measures targeting schools and gastronomy, with
275 reductions of -20.6% ($-21.2, -20.1$). This result emphasizes once more the necessity to protect
276 hospitals,⁴⁷ long-term care facilities⁴⁸ and other health and social institutions⁴⁹ as one of the first
277 lines of defense against SARS-CoV-2.

278 The NPI with the strongest effect size concerns public events with a reduction of -37.5
279 ($-38.6, -36.5$). In our dataset, this NPI also includes event bans, particularly on large unseated
280 indoor events. While public event bans have consistently been identified as one of most effective

281 NPIs, ⁴⁶ our effect size exceeds previous estimates which are maximally in the range of -25% . ⁴
282 This difference in effect sizes can be explained by the fact that our effect estimates are susceptible
283 to factors influencing the rapid rise in case numbers observed at the onset of the seasonal wave
284 in autumn 2020. It is feasible that the regional onset and early growth behaviour of this seasonal
285 wave was heavily driven by super-spreading events that have a disproportionate impact on regional
286 transmission rates while case numbers are still relatively low. Regions with event bans already in
287 place were not susceptible to such large increases in transmission rates in the early growth phase,
288 which might explain our rather large effect estimate.

289 We find a comparably small but significant transmission-increasing effect of mobility by
290 about 7.7% (95% CI 7.4, 8.0), even controlling for regional measures. While it is well-established
291 that mobility serves as a surrogate measure to quantify the effectiveness of the corresponding
292 NPI regime, ⁵⁰ our results indicate that telecommunications data derived mobility estimates might
293 capture additional behavioural differences.

294 Our work is subject to several limitations. As our parsimonious epidemiological modelling
295 approach was designed to be easy and robust to calibrate, it does not account for incubation periods,
296 distinguish between symptomatic and asymptomatic infections or contain undetected or quarantined
297 cases. More concrete, our estimates for the recovery time are much larger than the reported duration
298 of infectiousness. However, our recovery time should be understood as giving a time span within
299 which changes in NPIs or weather events might influence transmission rates. A recent analysis
300 reported that social distancing measures show a delayed impact of up to 18d to take full effect. ⁵¹

301 Hence our estimates for β effectively combine the incubation time and duration of infectiousness
302 with a delayed onset of NPI effectiveness. We also experimented with models that introduce an
303 additional variable for the delay between input time series and their effect on transmission rates.
304 This additional parameter did not result in substantial changes in model quality or effect sizes so we
305 removed it per Occam's razor.

306 In terms of limitations we further note that our approach cannot detect spatio-temporal
307 variations on finer scales than districts or days (e.g., whether rain is spread out over multiple hours
308 or in a short and intense burst) and that we do not address nonlinear dependencies or interaction
309 effects between individual input time series. There is also a number of NPIs that was implemented
310 much less than 50 times (e.g., regional quarantine measures) for which we could not estimate effect
311 sizes in a statistically robust way.

312 In conclusion, we find that regional differences in SARS-CoV-2 spread can in large parts be
313 explained by a combination of meteorological factors and regional NPIs. Our approach focuses
314 particularly on factors influencing the peak of the seasonal autumn 2020 wave in Austria, which
315 appears to be mostly driven by differences in temperature, cloudiness, humidity, and policies
316 targeting large public events. These findings have implications for what to expect for upcoming
317 seasonal SARS-CoV-2 waves. In particular, based on our results we would expect the next wave to
318 commence in regions where low mitigation measures targeting large public events combine with
319 shifts toward unfavourable environmental conditions. If no mitigation measures for public events
320 are in place, and precipitation, cloudiness and humidity move one SD in the direction of winter

321 conditions, our model expects transmission rates to be more than twice as high compared to a region
322 with control measures for public events and more favourable weather. While it has been previously
323 noted that epidemic forecasting is like weather forecasting due to uncertainties stemming from
324 nonlinear dynamics calibrated to noisy data streams,⁵² our results suggest that epidemic forecasting
325 to some extent *is* weather forecasting, with the added difficulty of needing to control for human
326 behaviour.

327 **5 Acknowledgments**

328 We thank Wolfgang Knecht for help with the figures. PK acknowledges financial support from
329 the Vienna Science and Technology Fund WWTF under MA16-045, from the Medizinisch-
330 Wissenschaftlichen Fonds des Bürgermeisters der Bundeshauptstadt Wien, no. CoVid004, and the
331 Austrian Science Promotion Agency FFG under 857136.

332 **6 Author Contributions**

333 KL and PK developed the analytical framework and analyzed the data. MK, JC, SL and CM
334 contributed to developing the analytical framework and analyzing the data. FW and CW curated the
335 weather data. KH, LK, SS and FB curated the NPI data. GH curated the mobility data. MB and NP
336 contributed to analyzing the weather data. KL, MK and PK wrote the first draft of the manuscript.
337 All authors reviewed and edited the manuscript. PK conceived and designed the study.

338 **7 References**

- 339 1. Haug, N., Geyrhofer, L., Londei, A. et al. Ranking the effectiveness of worldwide COVID-19
341 government interventions. *Nat Hum Behav* 4, 1303–1312 (2020).
- 342 2. Islam N, Sharp SJ, Chowell G, et al. Physical distancing interventions and incidence of coron-
343 avirus disease 2019: natural experiment in 149 countries. *BMJ* 370 (2020).
- 344 3. Brauner, JM, Mindermann S, Sharma M, et al. Inferring the effectiveness of government
345 interventions against COVID-19. *Science* 371, 6531 (2021).
- 346 4. Li Y, Campbelt H, Kulkarni D, et al. The temporal association of introducing and lifting non-
347 pharmaceutical interventions with the time-varying reproduction number (R) of SARS-CoV-2:
348 a modelling study across 131 countries. *The Lancet Infectious Diseases* 21(2), 193 (2021).
- 349 5. Plümper T, Neumayer E. The pandemic predominantly hits poor neighbourhoods? SARS-CoV-
350 2 infections and COVID-19 fatalities in German districts. *European Journal of Public Health*
351 30(6) 1176 (2020).
- 352 6. Buja A, Paganini M, Cocchio S, et al. Demographic and socio-economic factors, and healthcare
353 resource indicators associated with the rapid spread of COVID-19 in Northern Italy: An
354 ecological study. *PLoS One*, 15(12), e0244535 (2020).
- 355 7. Ehlert, A. The socio-economic determinants of COVID-19: a spatial analysis of German county
356 level data. *Socio-Economic Planning Sciences*, 101083 (2021).

- 357 8. Campbell, F, Archer, B, Laurenson-Schafer, H, et al. Increased transmissibility and global
358 spread of SARS-CoV-2 variants of concern as at June 2021. *Eurosurveillance*, 26(24), 2100509
359 (2021).
- 360 9. Gómez, CE, Perdiguero, B, Esteban, M. Emerging SARS-CoV-2 variants and impact in global
361 vaccination programs against SARS-CoV-2/COVID-19. *Vaccines*, 9(3), 243 (2021).
- 362 10. Moreno, GK, Braun, KM, Riemersma, KK, et al. Revealing fine-scale spatiotemporal differ-
363 ences in SARS-CoV-2 introduction and spread. *Nature Communications*, 11(1), 1-13 (2020).
- 364 11. Gross, B, Zheng, Z, Liu, S, et al. Spatio-temporal propagation of COVID-19 pandemics. *EPL*
365 (*Europhysics Letters*), 131(5), 58003 (2020).
- 366 12. Chen Y, Li Q, Karimian H, Chen X, Li X. Spatio-temporal distribution characteristics and
367 influencing factors of COVID-19 in China. *Sci Rep*. 2021 Feb 12;11(1):3717.
- 368 13. Menebo MM. Temperature and precipitation associate with Covid-19 new daily cases: A
369 correlation study between weather and Covid-19 pandemic in Oslo, Norway. *Sci Total Environ*.
370 2020 Oct 1;737:139659.
- 371 14. Ujiie M, Tsuzuki S, Ohmagari N. Effect of temperature on the infectivity of COVID-19. *Int J*
372 *Infect Dis*. 2020 Jun;95:301-303.
- 373 15. Pan J, Yao Y, Liu Z, Meng X, Ji JS, Qiu Y, Wang W, Zhang L, Wang W, Kan H. Warmer
374 weather unlikely to reduce the COVID-19 transmission: An ecological study in 202 locations
375 in 8 countries. *Sci Total Environ*. 2021 Jan 20;753:142272.

- 376 16. Smith TP, Flaxman S, Gallinat AS, Kinosian SP, Stemkovski M, et al. Temperature and popula-
377 tion density influence SARS-CoV-2 transmission in the absence of nonpharmaceutical interven-
378 tions. *Proceedings of the National Academy of Sciences USA*. 2021 Jun 22;118:e2019284118.
- 379 17. Briz-Redón Á, Serrano-Aroca Á. A spatio-temporal analysis for exploring the effect of temper-
380 ature on COVID-19 early evolution in Spain. *Sci Total Environ*. 2020 Aug 1;728:138811.
- 381 18. Badr HS, Du H, Marshall M, Dong E, Squire MM, Gardner LM. Association between mobility
382 patterns and COVID-19 transmission in the USA: a mathematical modelling study. *The Lancet*
383 *Infectious Diseases*. 2020 Nov 1;20:1247-1254.
- 384 19. Chang S, Pierson E, Koh PW, Gerardin J, Redbird B, Grusky D, Leskovec J. Mobility network
385 models of COVID-19 explain inequities and inform reopening. *Nature*, 2020 Nov 10;589:82-87.
- 386 20. Nouvellet P, Bhatia S, Cori A, Ainslie KEC, Baguelin M, et al. Reduction in mobility and
387 COVID-19 transmission. *Nature Communications*. 2021 Feb 17;12:1090.
- 388 21. Yechezkel M, Weiss A, Rejwan I, Shahmoon E, Ben-Gal S, Yamin D. Human mobility and
389 poverty as key drivers of COVID-19 transmission and control. *BMC Public Health*. 2021 Mar
390 25;21:596.
- 391 22. Althouse, BM, Wenger, EA, Miller, JC, et al. Superspreading events in the transmission
392 dynamics of SARS-CoV-2: Opportunities for interventions and control. *PLoS biology*, 18(11),
393 e3000897 (2020).

- 394 23. Popa, A, Genger, JW, Nicholson, MD, et al. Genomic epidemiology of superspreading events
395 in Austria reveals mutational dynamics and transmission properties of SARS-CoV-2. *Science*
396 *translational medicine*, 12(573) (2020).
- 397 24. Lemieux, JE, Siddle, KJ, Shaw, BM, et al. Phylogenetic analysis of SARS-CoV-2 in Boston
398 highlights the impact of superspreading events. *Science*, 371(6529) (2021).
- 399 25. Liu, Y, Eggo, RM, Kucharski, AJ. Secondary attack rate and superspreading events for SARS-
400 CoV-2. *The Lancet*, 395(10227), e47 (2020).
- 401 26. Seity, Y., Brousseau, P., Malardel, S., Hello, G., Bénard, P., Bouttier, F., Lac, C., Masson, V.
402 The AROME-France Convective-Scale Operational Model, *Monthly Weather Review*, 139(3),
403 976-991 (2011).
- 404 27. Termonia, P., Fischer, C., Bazile, E., Bouyssel, F., Brožková, R., Bénard, P., Bochenek, B.,
405 Degrauwe, D., Derková, M., El Khatib, R., Hamdi, R., Mašek, J., Pottier, P., Pristov, N., Seity,
406 Y., Smolíková, P., Španiel, O., Tudor, M., Wang, Y., Wittmann, C., and Joly, A.: The ALADIN
407 System and its canonical model configurations AROME CY41T1 and ALARO CY40T1, *Geosci.*
408 *Model Dev.*, 11, 257–281, <https://doi.org/10.5194/gmd-11-257-2018> (2018).
- 409 28. Petherick, A, Goldszmidt, RG, Andrade, EB, et al. A worldwide assessment of COVID-19
410 pandemic-policy fatigue. *Nature Human Behaviour* (2021).
- 411 29. Heiler G, Reisch T, Hurt J, Forgahani J, Omani A, et al. Country-wide mobility changes
412 observed using mobile phone data during COVID-19 pandemic. In 2020 IEEE International
413 Conference on Big Data (Big Data) (pp. 3123-3132). IEEE.

- 414 30. GOEG/AGES, Manual Corona-Kommission, https://corona-ampel.gv.at/sites/corona-ampel.gv.at/files/Manual%20Ampelsystem_3.0_bf.pdf,
415
416 accessed: 2021-08-04.
- 417 31. [https://www.ages.at/en/wissen-aktuell/publikationen/
418 epidemiologische-parameter-des-covid19-ausbruchs-oesterreich-2020/](https://www.ages.at/en/wissen-aktuell/publikationen/epidemiologische-parameter-des-covid19-ausbruchs-oesterreich-2020/),
419 accessed: 2021-08-04.
- 420 32. Brousseau, P., Berre, L., Bouttier, F. and Desroziers, G. Background-error covariances for a
421 convective-scale data-assimilation system: AROME–France 3D-Var. *Q.J.R. Meteorol. Soc.*,
422 137: 409-422. <https://doi.org/10.1002/qj.750> (2011)
- 423 33. Anderson, RM, May, RM. *Infectious diseases of humans: dynamics and control.* (Oxford
424 University Press, England, 1992).
- 425 34. Prem, K., Cook, A., and Jit, M.. Projecting social contact matrices in 152 countries using contact
426 surveys and demographic data. *PLOS Computational Biology*, 13(9):e1005697, 10.1371/journal.pcbi.1005697 (2017)
427
- 428 35. Liu, J., Zhou, J., Yao, J., Zhang, X., Li, L., Xu, X., He, X., Wang, B., Fu, S., Niu. T., Yan, J.,
429 Shi, Y., Ren, X., Niu, J., Zhu, W., Li, S., Luo, B., Zhang, K. Impact of meteorological factors
430 on the COVID-19 transmission: A multi-city study in China. *Science of The Total Environment*
431 (2020), 726, 138513, <https://doi.org/10.1016/j.scitotenv.2020.138513>
- 432 36. Ellwanger JH, Chies JAB. Wind: a neglected factor in the spread of infectious diseases. *Lancet*
433 *Planet Health*. 2018 Nov;2(11).

- 434 37. Pani SK, Lin NH, RavindraBabu S. Association of COVID-19 pandemic with meteorological
435 parameters over Singapore. *Sci Total Environ.* 2020;740:140112.
- 436 38. Guo C, Bo Y, Lin C, et al. Meteorological factors and COVID-19 incidence in 190 countries:
437 An observational study. *Sci Total Environ.* 2021;757:143783.
- 438 39. Gao, M, Zhou, Q, Yang, X, et al. Nonlinear modulation of COVID-19 transmission by climate
439 conditions. *Meteorological Applications*, 28(2), e1985 (2021).
- 440 40. Biryukov, J, Boydston, JA, Dunning, RA, et al. Increasing temperature and relative humidity
441 accelerates inactivation of SARS-CoV-2 on surfaces. *mSphere*, 5(4), e00441-20 (2020).
- 442 41. Dabisch, P, Schuit, M, Herzog, A, et al. The influence of temperature, humidity, and simulated
443 sunlight on the infectivity of SARS-CoV-2 in aerosols. *Aerosol Science and Technology*, 55(2),
444 142-153 (2021).
- 445 42. Kwon, T, Gaudreault, NN, Richt, JA. Environmental stability of SARS-CoV-2 on different
446 types of surfaces under indoor and seasonal climate conditions. *Pathogens*, 10(2), 227 (2021).
- 447 43. Ratnesar-Shumate, S, Williams, G, Green, B, et al. Simulated sunlight rapidly inactivates
448 SARS-CoV-2 on surfaces. *The Journal of infectious diseases*, 222(2), 214-222 (2020).
- 449 44. Schuit, M, Ratnesar-Shumate, S, Yolitz, J, et al. Airborne SARS-CoV-2 is rapidly inactivated
450 by simulated sunlight. *The Journal of infectious diseases*, 222(4), 564-571 (2020).

- 451 45. Gunthe, S.S., Swain, B., Patra, S.S. et al. On the global trends and spread of the COVID-19
452 outbreak: preliminary assessment of the potential relation between location-specific temperature
453 and UV index. *J Public Health (Berl.)* (2020). <https://doi.org/10.1007/s10389-020-01279-y>
- 454 46. Mendez-Brito, A, El Bcheraoui, C, Pozo-Martin, F. Systematic review of empirical studies
455 comparing the effectiveness of non-pharmaceutical interventions against COVID-19. *Journal of*
456 *Infection*, <https://doi.org/10.1016/j.jinf.2021.06.018> (2021).
- 457 47. Xiang, B, Li, P, Yang, X, et al. The impact of novel coronavirus SARS-CoV-2 among healthcare
458 workers in hospitals: An aerial overview. *American journal of infection control*, 48(8), 915-917
459 (2020).
- 460 48. Krutikov, M, Hayward, A, Shallcross, L. Spread of a variant SARS-CoV-2 in long-term care
461 facilities in England. *New England Journal of Medicine*, 384(17), 1671-1673 (2021).
- 462 49. Lee, EC, Wada, NI, Grabowski, MK, et al. The engines of SARS-CoV-2 spread. *Science*,
463 370(6515), 406-407 (2020).
- 464 50. García-Cremades, S, Morales-García, J, Hernández-Sanjaime, R, et al. Improving prediction of
465 COVID-19 evolution by fusing epidemiological and mobility data. *Scientific Reports*, 11(1),
466 1-16 (2021).
- 467 51. Nader, IW, Zeilinger, EL, Jomar, D, Zauchner, C. Onset of effects of non-pharmaceutical
468 interventions on COVID-19 infection rates in 176 countries. *BMC Public Health*, 21(1), 1-7
469 (2021).

470 52. Moran, KR, Fairchild, G, Generous, N, et al. Epidemic forecasting is messier than weather
471 forecasting: the role of human behavior and internet data streams in epidemic forecast. The
472 Journal of infectious diseases, 214, 404-408 (2016).